Subnuclear positioning and interchromosomal clustering of the *GAL1-10* locus are controlled by separable, interdependent mechanisms

Donna Garvey Brickner[a], Varun Sood[a], Evelina Tutucci[b], Robert Coukos[a], Kayla Viets[a,†], Robert H. Singer[b,c], and Jason H. Brickner[a,*]

[a]Department of Molecular Biosciences, Northwestern University, Evanston, IL 60208; [b]Department of Anatomy and Structural Biology, Albert Einstein College of Medicine, Bronx, NY 10461; [c]Janelia Research Campus, Howard Hughes Medical Institute, Ashburn, VA 20147

ABSTRACT **On activation, the *GAL* genes in yeast are targeted to the nuclear periphery through interaction with the nuclear pore complex. Here we identify two *cis*-acting "DNA zip codes" from the *GAL1-10* promoter that are necessary and sufficient to induce repositioning to the nuclear periphery. One of these zip codes, GRS4, is also necessary and sufficient to promote clustering of *GAL1-10* alleles. GRS4, and to a lesser extent GRS5, contribute to stronger expression of *GAL1* and *GAL10* by increasing the fraction of cells that respond to the inducer. The molecular mechanism controlling targeting to the NPC is distinct from the molecular mechanism controlling interchromosomal clustering. Targeting to the nuclear periphery and interaction with the nuclear pore complex are prerequisites for gene clustering. However, once formed, clustering can be maintained in the nucleoplasm, requires distinct nuclear pore proteins, and is regulated differently through the cell cycle. In addition, whereas targeting of genes to the NPC is independent of transcription, interchromosomal clustering requires transcription. These results argue that zip code–dependent gene positioning at the nuclear periphery and interchromosomal clustering represent interdependent phenomena with distinct molecular mechanisms.**

Monitoring Editor
Tom Misteli
National Cancer Institute, NIH

Received: Mar 17, 2016
Revised: Jul 22, 2016
Accepted: Jul 27, 2016

INTRODUCTION

Eukaryotic genomes, from fungi to humans, are spatially organized (Meldi and Brickner, 2011). Budding yeast arranges its chromosomes in the "Rabl conformation," with centromeres associated with the spindle pole body and telomeres clustered at the nuclear periphery opposite the nucleolus (Zimmer and Fabre, 2011). In differentiated metazoan cells, chromosomes fold back on themselves, producing distinct "territories" (Cremer *et al.*, 2006). The spatial position of individual genes is also nonrandom, and coregulated genes can cluster together within the nucleus. The spatial arrangement of genes and chromosomes correlates with transcriptional programs, changing between developmental stages and in disease states (Parada *et al.*, 2002; Meaburn *et al.*, 2009, 2016; Leshner *et al.*, 2016). This suggests that changes in global nuclear architecture are either a cause or an effect of different transcriptional programs.

Although the molecular mechanisms that influence the spatial arrangement of the genome are still being discovered, several results suggest that the genome encodes its spatial organization through recognition of *cis*-acting DNA elements by sequence-specific DNA-binding proteins. Transcription factors influence local chromatin structure and transcriptional activity, which can lead to changes in the subnuclear positioning of genes (Ragoczy *et al.*, 2006; Rohner *et al.*, 2013; Gonzalez-Sandoval *et al.*, 2015). In addition, DNA-binding "architectural" proteins control the intramolecular folding and looping of chromosomes into topologically isolated domains (Dixon *et al.*, 2012; Nora *et al.*, 2012; Jin *et al.*, 2013; Phillips-Cremins *et al.*, 2013; Rao *et al.*, 2014). Finally, the positioning of genes with respect to nuclear landmarks and the clustering of

This article was published online ahead of print in MBoC in Press (http://www.molbiolcell.org/cgi/doi/10.1091/mbc.E16-03-0174) on August 3, 2016.

†Present address: Department of Biology, Johns Hopkins University, Baltimore, MD 21218.

*Address correspondence to: Jason Brickner (j-brickner@northwestern.edu).

Abbreviations used: GRS, gene recruitment sequence; MLP, myosin-like protein; NPC, nuclear pore complex; OP, 1,10-*o*-phenanthroline.

Supplemental Material can be found at:
http://www.molbiolcell.org/content/suppl/2016/08/01/mbc.E16-03-0174v1.DC1.html

genes depend on *cis*-acting DNA elements, their corresponding DNA-binding proteins, and/or chromatin modifications (Ahmed *et al.*, 2010; Light *et al.*, 2010, 2013; Zullo *et al.*, 2012; Bian *et al.*, 2013; Kind *et al.*, 2013; Gonzalez-Sandoval *et al.*, 2015; Harr *et al.*, 2015). These observations suggest that the sequence and chromatin state of the genome influence its spatial organization.

The spatial organization of the genome within the nucleus can be dynamically altered by developmental or environmental cues. During differentiation in metazoan systems, induced genes often move away from the nuclear lamina to a more nucleoplasmic position, and silenced genes often move to the nuclear lamina (Guelen *et al.*, 2008; Luperchio *et al.*, 2014; Lemaitre and Bickmore, 2015). However, many inducible genes move from the nucleoplasm to the nuclear periphery upon activation in yeast (Brickner and Walter, 2004; Casolari *et al.*, 2004, 2005; Randise-Hinchliff *et al.*, 2016). In *Drosophila*, *Caenorhabditis elegans*, mouse, and human cells, thousands of genes interact with nuclear pore proteins (Brown *et al.*, 2008; Capelson *et al.*, 2010; Kalverda *et al.*, 2010; Liang *et al.*, 2013; Rohner *et al.*, 2013). The interaction of genes with nuclear pore proteins in metazoan nuclei can occur both at the nuclear periphery, in association with the nuclear pore complex (NPC), or in the nucleoplasm, in association with soluble nuclear pore proteins (Brown *et al.*, 2008; Capelson *et al.*, 2010; Kalverda *et al.*, 2010; Liang *et al.*, 2013; Light *et al.*, 2013). Thus, although the interactions occur in a different location, they may represent a conserved mechanism. In yeast, repositioning to the nuclear periphery involves a physical interaction with the NPC and requires transcription factors, components of the NPC, mRNA transport factors, the SAGA histone acetyltransferase complex, and Mediator (Cabal *et al.*, 2006; Dieppois *et al.*, 2006; Ahmed *et al.*, 2010; Schneider *et al.*, 2015; Randise-Hinchliff *et al.*, 2016). Thus interaction with the NPC is coordinated with transcription and mRNA export.

Transcription and repositioning to the nuclear periphery can be uncoupled. Where it is understood, the movement of yeast genes to the NPC is mediated by *cis*-acting DNA elements found in their promoters and can occur independent of transcription of the locus and RNA polymerase II activity (Brickner *et al.*, 2007, 2012; Ahmed *et al.*, 2010; Light *et al.*, 2010; Randise-Hinchliff *et al.*, 2016). For example, the targeting of the *INO1* gene to the nuclear periphery is controlled by two *cis*-acting gene recruitment sequences (GRS1 and GRS2) in the promoter. The GRS elements are distinct from the elements required for transcriptional activity (the UAS_{INO} elements) and the GRSs are both necessary for *INO1* localization at the nuclear periphery and sufficient to cause peripheral localization of an ectopic site. Thus we refer to such elements as "DNA zip codes." We have identified such elements in the promoters of several genes and, in several cases, the transcription factors that bind to them to mediate targeting to the NPC (Brickner *et al.*, 2012; Randise-Hinchliff *et al.*, 2016). The repositioning of inducible genes to the nuclear periphery is rapid, occurring within 15–60 min, and is controlled through transcription factor binding or transcription factor function (Brickner *et al.*, 2007; Randise-Hinchliff *et al.*, 2016).

Coregulated genes can cluster together within the nucleus, and this may serve to compartmentalize the nucleus or regulate gene expression (Pombo *et al.*, 2000; Brown *et al.*, 2006). During embryogenesis in *Drosophila*, silenced Polycomb-regulated loci cluster together (Cheutin and Cavalli, 2012). During hematopoiesis, the hemoglobin genes (*Hba* and *Hbb*) cluster with coregulated genes through a mechanism that requires the transcriptional activator Klf1 (Schoenfelder *et al.*, 2010). Similarly, hundreds of tRNA genes throughout the yeast genome converge into distinct foci near the nucleolus (Thompson *et al.*, 2003; Haeusler *et al.*, 2008; Rodley *et al.*, 2011). Finally, yeast genes that share DNA zip codes cluster together in association with the nuclear periphery (Brickner *et al.*, 2012; Randise-Hinchliff *et al.*, 2016). For example, the active *INO1* gene clusters together with other GRS1-targeted genes at the nuclear pore complex, which requires both the GRS1-binding transcription factor Put3 and components of the NPC (Brickner *et al.*, 2012, 2015).

In this article, we explore the changes in spatial organization of the yeast nucleus induced in response to growth in galactose. The peripheral recruitment of the *GAL1-10* gene is controlled by two redundant GRS elements (GRS4 and GRS5) in the promoter and requires NPC proteins. The GRS4 promotes stronger transcription of *GAL1* and *GAL10* by increasing the fraction of cells that respond to galactose. Furthermore, GRS4 mediates interallelic interchromosomal clustering of active *GAL1-10* alleles. Clustering requires an overlapping but distinct set of NPC proteins from those required for targeting to the nuclear periphery. Although recruitment of *GAL1-10* to the nuclear periphery does not require transcription, the establishment of *GAL1-10* interchromosomal clusters does require transcription. Both peripheral positioning and interchromosomal clustering are dynamically regulated through the cell cycle. The cell cycle regulation of clustering is linked to the regulation of peripheral localization, but the two phenomena show different phases. Thus the subnuclear positioning and interchromosomal clustering of *GAL1-10* are mediated by separate but interdependent mechanisms.

RESULTS

DNA zip codes in the *GAL1-10* promoter are necessary and sufficient to promote targeting to the nuclear periphery

To determine whether *GAL1-10* recruitment to the nuclear periphery requires *cis*-acting DNA elements, we used a chromatin localization assay. An array of 128 Lac operator sites (LacO array) was integrated downstream of *GAL1* in a strain coexpressing the Lac repressor fused to green fluorescent protein (GFP-LacI) and an endoplasmic reticulum membrane protein tagged with mCherry (Egecioglu *et al.*, 2014). Live cells were imaged by confocal microscopy and scored as either peripheral (i.e., the GFP dot overlaps the nuclear membrane) or nucleoplasmic (Figure 1A). When repressed in glucose medium, *GAL1-10* occupies a primarily nucleoplasmic distribution (36 ± 3% peripheral; expect ~30% of the nucleus to be unresolvable from the nuclear envelope; Brickner and Walter, 2004). In galactose medium, the active *GAL1-10* gene repositions to the nuclear periphery (71 ± 3% peripheral; Figure 1B). In contrast, the *URA3* locus localizes in the nucleoplasm in both glucose and galactose media (Figure 1B). To test whether targeting to the nuclear periphery is controlled by *cis*-acting DNA elements, we inserted the 667–base pair *GAL1-10* promoter beside *URA3* and scored for peripheral localization. The promoter was sufficient to recruit *URA3* to the nuclear periphery specifically in galactose (64 ± 4% peripheral; Figure 1B). Furthermore, deletion of the *GAL1-10* promoter at the endogenous location blocked targeting to the periphery (Figure 1C). This suggested that the *GAL1-10* promoter contains *cis*-acting DNA elements that promote localization to the nuclear periphery.

To identify DNA elements that function as zip codes within the *GAL1-10* promoter, we inserted a series of overlapping promoter fragments at *URA3* and tested them for their ability to target the ectopic locus to the nuclear periphery. We repeated this process iteratively to identify minimal DNA elements that function as DNA zip codes. We identified two DNA elements from the *GAL1-10* promoter, gene recruitment sequences 4 (GRS4; 5′-TATATTGA-3′) and 5 (GRS5; 5′-CTTTCA-3′), which were able to reposition *URA3* to the nuclear periphery, independent of orientation (Figure 1B). These elements are

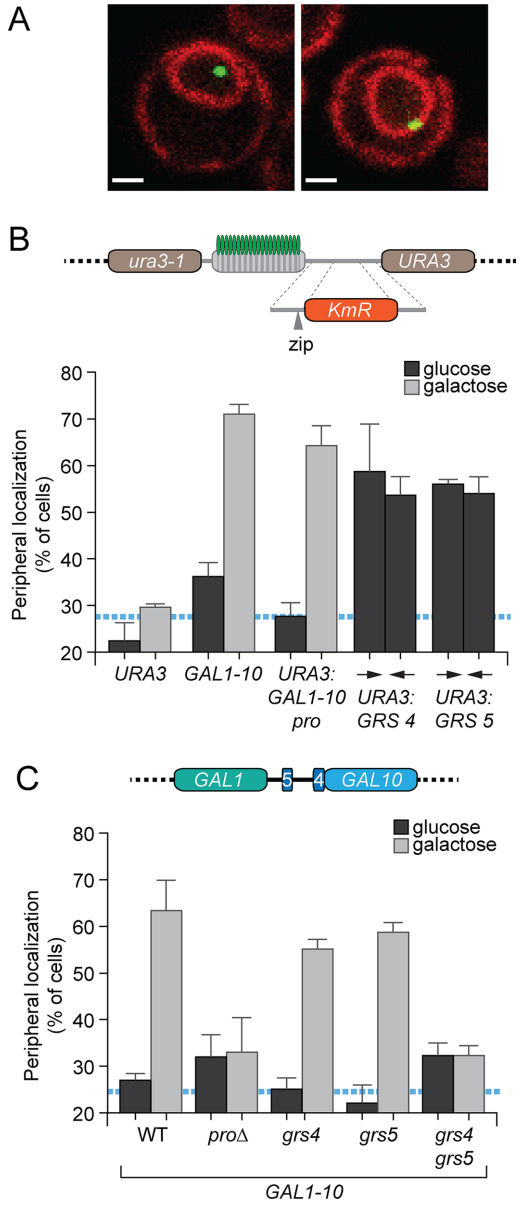

FIGURE 1: *GAL1-10* promoter contains information necessary and sufficient for recruitment to the nuclear periphery. (A) Merged confocal micrographs of yeast cells expressing LacI-GFP (green) and mCherryER04 (red). An array of 128 Lac repressor binding sites (LacO array) was integrated 3′ of the *GAL1* gene. Left, cell scored as nucleoplasmic; right, cell scored as peripheral. Scale bar, 1 μm. In B and C, cells in a population were scored as either nucleoplasmic or peripheral, and the mean of at least three biological replicates of 30–50 cells each is plotted (error bars are SEM). A blue, hatched line represents the fraction of the nucleus that is unresolvable from the nuclear envelope by light microscopy (Brickner and Walter, 2004; Egecioglu *et al.*, 2014). (B) Top, schematic of the *GAL1-10* promoter, highlighting the positions of GRS4 and GRS5. Bottom, strains containing the lac repressor array and either the 667–base pair *GAL1* promoter + ORF, the *GAL1-10* promoter alone, or the minimal GRS4 or GRS5 elements inserted in either orientation were grown in glucose or galactose medium and scored for peripheral localization. The endogenous *GAL1-10* locus was scored for comparison. (C) Cells with the LacO array integrated 3′ of the endogenous *GAL1* locus but lacking the *GAL1-10* promoter or with the GRS4 or GRS5 sequences mutated were grown in glucose or galactose and scored as nucleoplasmic or at the nuclear periphery.

distinct from the Gal4 transcription factor–binding sites, and targeting by these elements was constitutive, suggesting that additional elements in the endogenous promoter block GRS4 and GRS5-mediated peripheral targeting in glucose (Randise-Hinchliff *et al.*, 2016; see later discussion). Thus GRS4 and GRS5 function as DNA zip codes that are sufficient to promote peripheral targeting of an ectopic site.

To test whether GRS4 and GRS5 are necessary for *GAL1-10* recruitment to the nuclear periphery, we introduced transversion mutations into the GRS elements within the endogenous *GAL1-10* and assessed its localization. Neither the *grs4* nor the *grs5* mutation alone blocked relocalization to the nuclear periphery (Figure 1C). However, the *grs4 grs5* double mutation blocked repositioning to the nuclear periphery (Figure 1C). This indicates that the GRS4 and GRS5 elements redundantly control positioning of the *GAL1-10* locus to the nuclear periphery.

The GRS4 and GRS5 zip codes enhance *GAL1-10* transcription

To understand how the interaction of *GAL1-10* with the NPC affects gene expression, we measured mRNA production and transcription from the *GAL1-10* promoter mutated for GRS4, GRS5, and both, using several different assays. First, the *GAL1* and *GAL10* mRNA abundance was quantified relative to *ACT1* by reverse transcriptase quantitative PCR (RT-qPCR) over time after shifting cells to galactose from either glucose (a repressing carbon source; Figure 2, A–C) or raffinose (a nonrepressing carbon source; Figure 2, D–F). As a control, we also measured the accumulation of *GAL2* mRNA. Whereas mutation of the GRS5 had very little effect on expression of *GAL1* or *GAL10* (Figure 2, A–F), mutation of the GRS4 resulted in a clear defect in the expression of *GAL10* (Figure 2, B and E) and a weaker effect on the expression of *GAL1* (Figure 2, A and D), which was strongest in cells shifted from raffinose to galactose (Figure 2, D and E). The *grs4 grs5* mutant showed the strongest defect in the expression of *GAL1* and *GAL10* under both conditions. These mutations had no effect on the expression of *GAL2* (Figure 2, C and F). Therefore GRS4 promotes stronger expression of *GAL1* and *GAL10* in-*cis*. In the absence of GRS4, the GRS5 promotes expression of these genes to a lesser extent.

To confirm these results and test whether these mutations altered the structures of the mature *GAL1* or *GAL10* mRNAs, we performed Northern blot analysis in wild-type and *grs4* mutant strains after shifting cells from glucose to galactose for 6 h (Figure 2, G and H). Both *GAL1* and *GAL10* levels were decreased in the *grs4* mutant strain, but the levels of *GAL2*, *GAL3*, and *GAL7* were unaffected (Figure 2, G and H). We observed no changes in the mobility of any of these mRNAs in the *grs4* mutant strain, suggesting that this mutation does not have a dramatic effect on their termination or polyadenylation.

As an alternative method to test whether the changes in *GAL1* mRNA abundance were due to changes in transcription, we used single-molecule RNA fluorescent in situ hybridization (FISH) to quantify the number of cells in which *GAL1* is being transcribed, the nascent transcripts at the transcription site, and the number of mRNAs per cell after shifting from glucose to galactose for 2.5 h (Figure 2I; Zenklusen *et al.*, 2008). The fraction of cells having a *GAL1* transcription site (Figure 2J, left) or measurable *GAL1* mRNA (Figure 2J, right) was significantly reduced in the *grs4* and *grs4 grs5* mutant cells. Consistent with this observation, chromatin immunoprecipitation against RNA polymerase II suggested that the recruitment of RNAPII to the *GAL1-10* promoter was reduced in strains in which GRS4 was mutated (Supplemental Figure S1). However, among the cells that were transcribing *GAL1*, the *grs4* and *grs4 grs5*

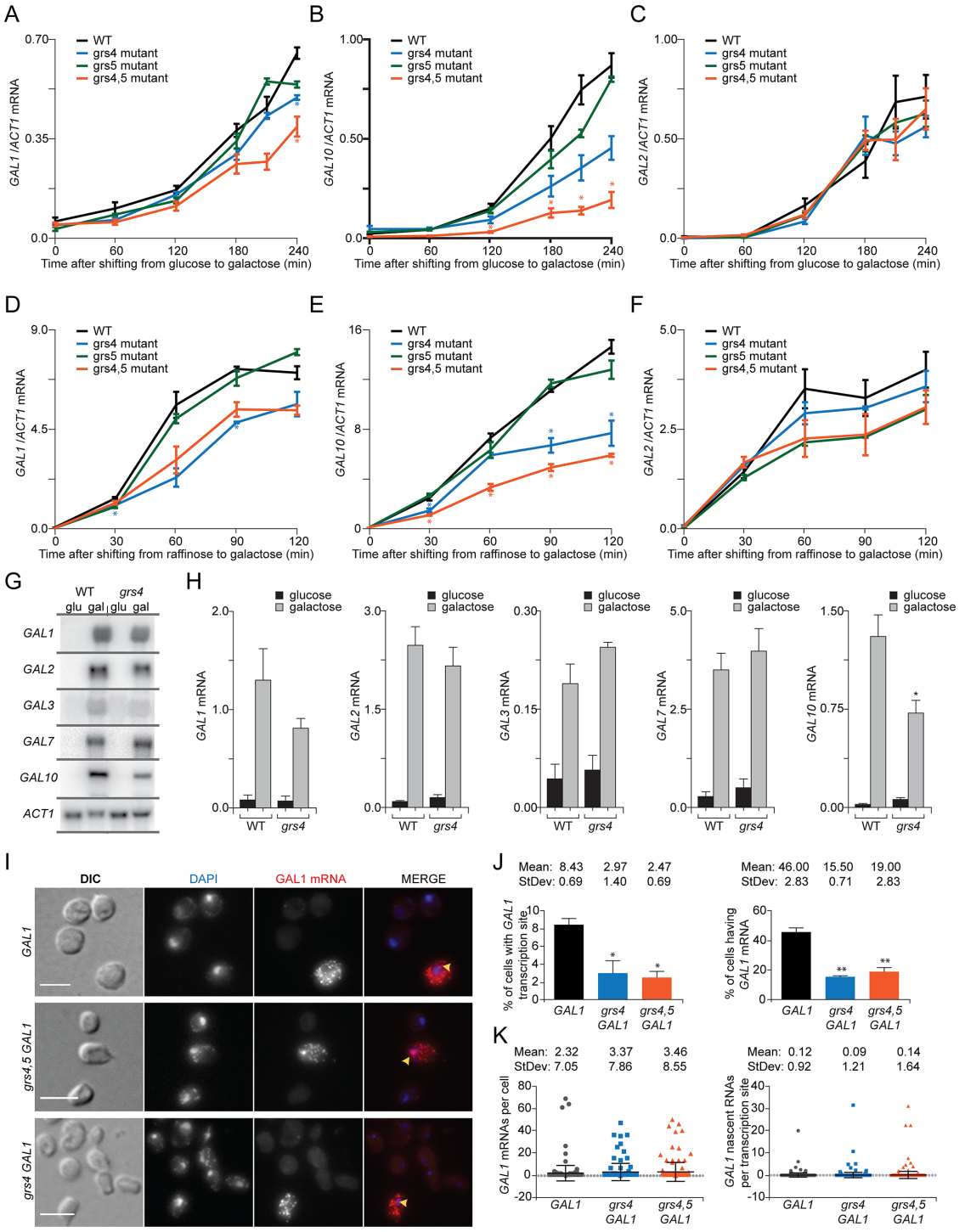

FIGURE 2: GRS4 promotes stronger transcription of *GAL1-10* by increasing the fraction of cells that induce the gene. (A–F) RT-qPCR measurements of the levels of *GAL1* (A,D), *GAL10* (B, E), and *GAL2* (C, F) mRNA relative to *ACT1* mRNA from wild-type (WT), *grs4*, or *grs4 grs5* cells shifted from glucose to galactose (A–C) or raffinose to galactose (D–F). (G) Northern blot analysis of *GAL* gene transcripts from WT and *grs4* mutant yeast strains grown in glucose or shifted to galactose for 6 h. Equal amount of total RNA was loaded, incubated with the indicated ^{32}P-labeled probes, and exposed to a phosphoimager screen. (H) Three experiments performed as described in G were quantified using ImageJ software. Data presented are the average signal intensity normalized to *ACT1* ± SEM. For A–H, *$p < 0.05$ comparing to WT using Student's *t* test. (I) Single-molecule RNA FISH against *GAL1* from WT, *grs4*, and *grs4 grs5* mutant strains. Differential contrast (DIC), DAPI staining, and *GAL1* RNA signals are shown in separate channels and merged. Arrowhead: site of transcription. Scale bar, 5 µm. (J, K) Quantification of percentage of cells with a *GAL1* transcription site (J, left), percentage of cells with measurable *GAL1* RNA (J, right), number of *GAL1* mRNAs per cell (K, left), and number of nascent *GAL1* RNAs per transcription site (K, right). For J and K, *$p < 0.05$ and **$p < 0.01$, Dunnett's multiple comparison test.

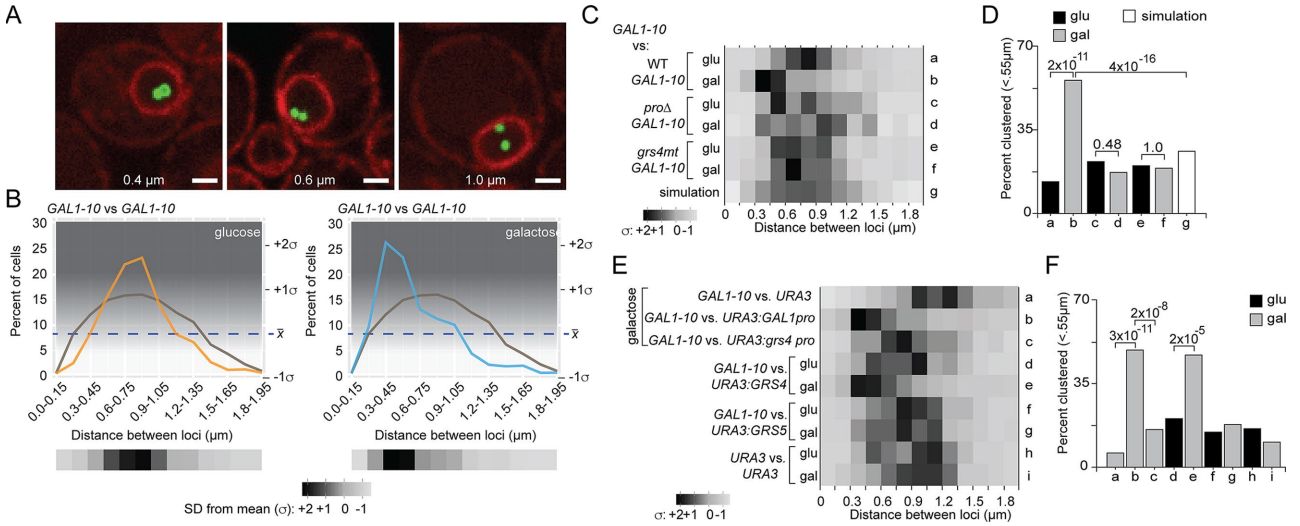

FIGURE 3: Interchromosomal clustering of *GAL1-10* genes is mediated by DNA zip codes. (A) Representative merged confocal images of diploid yeast cells expressing LacI-GFP (green), mCherry localized to the nuclear envelope and the endoplasmic reticulum (pER04, red; Egecioglu *et al.*, 2014), and having a LacO array integrated 3′ of both alleles of *GAL1*. Micrographs depict *GAL1-10* loci ~0.4 μm (left), 0.6 μm (center), and 1.0 μm (right) apart. Scale bar, 1 μm. (B) Diploid cells with both copies of the *GAL1-10* alleles tagged with the LacO array were grown overnight in glucose (left) or galactose (right), and the distance between the loci was measured for ≥100 cells and binned into 0.15-μm classes (top). Percentage of cells in each bin is plotted. For comparison, a simulation of the distribution of distances between two spots is shown (brown line; see *Materials and Methods*). Bottom, fraction of cells in each bin was compared with mean fraction of cells in each bin (hatched line) and the number of SDs from the mean (σ) is plotted as a heat map (according to the color scale). (C) Cells having the LacO array at both the WT allele and each of the indicated alleles of *GAL1-10* were grown overnight in glucose or galactose. The distance between the loci was measured and plotted as described in A. (D) From the distributions in C, percentage of the population in which the two alleles clustered together (<0.55 μm). The *p* values are based on a Fisher exact test. (E) Cells with one endogenously tagged *GAL1-10* locus and the WT or *grs4* mutant *GAL1-10* promoter or the GRS4 or GRS5 zip codes integrated at *URA3* were grown in glucose or galactose medium. The distance between the two loci was measured and analyzed as in C. (F) From the distributions in D, percentage of the population in which the two alleles clustered together (<0.55 μm). The *p* values are based on a Fisher exact test.

mutations did not significantly affect the number of *GAL1* mRNAs per cell (Figure 2K, left) or the number of nascent RNAs per transcription site (Figure 2K, right). Therefore we conclude that the GRS4 promotes stronger *GAL1-10* expression by increasing the fraction of cells that transcribe the locus in response to galactose. In the absence of GRS4, GRS5 can promote transcription, but in the wild-type *GAL1-10* promoter, GRS4 is the dominant element.

Interchromosomal clustering of *GAL1-10* alleles is controlled by GRS4

Hi-C chromosome capture of the yeast genome suggested that the *GAL* genes cluster together (Gehlen *et al.*, 2012). Furthermore, interaction between two ectopic copies of the *GAL1-10* promoter leads to interallelic transcriptional regulation in-*trans* (Zhang and Bai, 2016). These observations suggest that, like other NPC-associated genes, the *GAL* genes might exhibit interchromosomal clustering. To test this hypothesis, we generated a diploid yeast strain having both *GAL1-10* alleles marked with the LacO array (Figure 3A). We then measured the distances between the two alleles in a population of cells grown in either glucose or galactose, binned them into 0.15-μm bins, and plotted the distribution within the population (*Materials and Methods*; Figure 3B). For comparison, we also generated a simulation of the distribution of distances between two randomly localized, diffraction-limited spots in a population of cells. The simulation gave a broad distribution with a mean distance of 0.84 ± 0.38 μm (Figure 3B, brown line; *Materials and Methods*). In cells grown in glucose, we observed a narrower distribution, with a mean distance between the two alleles of 0.79 ± 0.28 μm, but this distribution was not significantly different from the simulation ($p = 0.12$; Wilcoxon rank sum test). However, in cells grown in galactose, the distribution of distances between the two alleles of *GAL1-10* shifted to shorter distances, with a mean distance of 0.61 ± 0.30 μm (Figure 3B, right). This shift is highly significant compared with either the simulated random distribution ($p = 2 \times 10^{-16}$) or the distribution from the glucose-grown cells ($p = 2 \times 10^{-11}$; Wilcoxon rank sum test). Thus, like *INO1*, *TSA2*, *HSP104*, *PRM1*, and *HIS4* (Brickner *et al.*, 2012; Randise-Hinchliff *et al.*, 2016), the *GAL1-10* locus undergoes interchromosomal, interallelic clustering upon activation.

To facilitate comparison among numerous conditions or strains, we developed a heat map representation for the distribution of distances (Figure 3B, bottom). The average percentage of cells per bin is ~7.7% (100% divided equally into 13 bins; hatched line in Figure 3B). For each bin, we calculated the number of standard deviations (σ) above or below this mean value ($\bar{X}$), expressed using a white–black color scale (Figure 3, B and C). From each distribution, we also calculated the fraction of cells in which the two alleles were "clustered," meaning that the distance between them was <0.55 μm (Figure 3D). The fraction of *GAL1-10* alleles that were <0.55 μm apart in glucose was 21% (Figure 3D, bar a), similar to the fraction <0.55 μm in the simulation (26%; Figure 3D, bar g; $p = 0.23$). In galactose, the fraction of *GAL1-10* alleles that were <0.55 μm apart

increased to 54% (Figure 3D, bar b), significantly greater than either the random simulation ($p = 4 \times 10^{-16}$, Fisher exact test) or the glucose condition ($p = 2 \times 10^{-11}$, Fisher exact test). Thus these two metrics (used here and later) reveal that *GAL1-10* alleles exhibit a significant shift toward shorter interallelic distances between cells grown in glucose and cells grown in galactose.

To explore the specificity of interchromosomal clustering and the role of DNA signals in this process, we examined the distribution of distances between wild-type *GAL1-10* and *GAL1-10* either lacking the promoter or lacking the GRS4. Either deletion of the promoter from one of the two alleles or mutation in the GRS4 at one allele blocked interallelic clustering, resulting in similar distributions in glucose and galactose (Figure 3, C and D). To test whether the *GAL1-10* promoter is sufficient to promote clustering with the endogenous *GAL1-10* locus, we measured the distance between *GAL1-10* and *URA3*, *URA3:GAL1-10pro*, or *URA3:GAL1-10pro grs4* mutant (Figure 3, E and F). *URA3* did not show significant clustering with itself or *GAL1-10*, giving a mean distance of 1.23 ± 0.42 µm and 6% with <0.55 µm (Figure 3, E and F, bars a, h, and i). However, introduction of the *GAL1-10* promoter at *URA3* led to a highly significant increase in clustering in galactose, giving a mean distance of 0.66 ± 0.31 µm and 47% with <0.55 µm (Figure 3, E and F, bars a and b). Mutation of the GRS4 dramatically reduced clustering (mean distance of 0.92 ± 0.34 µm and11% with <0.55 µm; Figure 3, E and F, bar c). Therefore the GRS4 is necessary for interchromosomal clustering of *GAL1-10* alleles both at the endogenous locus and between an endogenous locus and an ectopic site.

To test whether GRS4 or GRS5 alone is sufficient to induce interchromosomal clustering with *GAL1-10*, we measured the distances between *GAL1-10* and either *URA3:GRS4* or *URA3:GRS5* (GRS4 or GRS5 inserted at *URA3:LacO*; Egecioglu *et al.*, 2014) in glucose and galactose. In glucose, *GAL1-10* clustered with neither *URA3:GRS4* nor *URA3:GRS5* (Figure 3, E and F, bars d and f). However, in cells grown in galactose, *GAL1-10* clustered strongly with *URA3:GRS4* (mean distance of 0.64 ± 0.28 µm and 47% with <0.55 µm; Figure 3, E and F, bar e) but not with *URA3:GRS5* (mean distance of 0.86 ± 0.31 µm and 18% with <0.55 µm; Figure 3, E and F, bar g). Therefore the GRS4 sequence is necessary and sufficient to induce interchromosomal clustering with *GAL1-10*. However, GRS5 is restricted to a role in peripheral recruitment and has no apparent role in interchromosomal clustering. This suggests that targeting to the periphery is not sufficient to lead to interchromosomal clustering.

Dynamics of *GAL1-10* interchromosomal clustering

We next explored the dynamics of *GAL1-10* clustering and peripheral targeting in live cells. In diploid cells having both alleles of *GAL1-10* marked with the LacO array (Figure 3A), we scored both recruitment to the nuclear periphery and interallelic clustering (Figure 4A). After switching cells from glucose to galactose, we sampled a population of cells every 5 min for 15 min and every 15 minutes thereafter for 2 h. To follow the peripheral positioning of two alleles, we scored them in two ways. For Figure 4A, we quantified the fraction of alleles in the population that colocalized with the nuclear envelope (blue line), as well as the fraction of cells in which the two alleles are <0.55 µm (red line). For Figure 4B, we scored the fraction of cells in which both alleles were peripheral (orange), the fraction of cells in which both alleles were nucleoplasmic (cyan), and the fraction of cells in which the two alleles were <0.55 µm (gray). Consistent with our previous work with fixed cells, repositioning to the nuclear periphery was a time-dependent reaction that reached maximal levels after 15 min in galactose (Brickner *et al.*, 2007). This corresponded to a shift from ~30 to ~ 70% of the alleles in the population colocalized with the nuclear envelope (Figure 4A, blue circles). In glucose, we observed >50% of the cells having both alleles in the nucleoplasm and <10% having both alleles at the periphery (Figure 4B). After shifting to galactose for 15 min, the fraction of cells in which both alleles were nucleoplasmic dropped to ~20% (Figure 4B, cyan), and the fraction of cells in which both alleles were peripheral increased to ~40% (Figure 4B, orange). This suggests that the targeting of the two alleles is somewhat coordinated. The clustering of *GAL1-10* alleles increased more slowly than peripheral localization after shifting to galactose, increasing from ~10% to ~50% over 1 h (Figure 4, A and B). This is consistent with the idea that clustering occurs after both *GAL1-10* alleles are recruited to the nuclear periphery.

We also analyzed the distances between *GAL1-10* alleles over time in living cells, using spinning-disk confocal movies of single cells. In both the cells grown in glucose and the cells grown in galactose, we observed a range of distances between *GAL1-10* alleles in such movies, ranging from 0.15 to 1.8 µm (Figure 4C). However, three differences were clear. First, in glucose, we observed a broad, continuous range of distances between the alleles, whereas in galactose, we observed two distinct populations. In one population, the two alleles were close to each other (<0.55 µm), and in the other, they were far apart (>0.55 µm; Figure 4C). Second, the variance of the distances between *GAL1-10* alleles within each cell, measured as the distribution of step sizes between consecutive time points, was significantly greater in cells grown in glucose than in cells grown in galactose (Figure 4C, $p = 2 \times 10^{-4}$, Student's *t* test). Third, when we quantified the fraction of the time points during which *GAL1-10* alleles were <0.55 µm in cells grown in glucose, a majority of these close interactions were brief (Figure 4D, black bars). However, in cells grown in galactose, the duration of the interactions showed a clear bimodal distribution, resulting in a decrease in the fraction of cells in which the alleles were within 0.55 µm for ≤40% of the time points and an increase in the fraction in which the alleles were within 0.55 µm for ≥50% of the time points (Figure 4D). Thus populations of cells in which the *GAL1-10* alleles are clustered were readily distinguishable from populations of cells in which they are not.

The bimodal nature of the population was clear when single cells were analyzed over time but was not obvious from instantaneous measurements of populations (Figure 3B). To compare the data acquired from individual cells over time to the single–time point experiments, we pooled the distances for all of the time points from all of the cells in either glucose or galactose and analyzed their distribution as in Figure 3 (Figure 4F). The pooled data for 20 cells in glucose and galactose over 20 time points recapitulated the patterns we observed using a single time point for 100 cells (Figure 4F). This indicates that our method and data analysis are robust and that the behavior of individual cells over time is consistent with single–time point measurements of an asynchronous population.

Peripheral targeting and interchromosomal clustering require overlapping but distinct nuclear pore components

Genes that are recruited to the nuclear periphery physically associate with the nuclear pore, and loss of a number of nuclear pore proteins blocks repositioning to the periphery (Cabal *et al.*, 2006; Dieppois *et al.*, 2006; Brickner *et al.*, 2007; Ahmed *et al.*, 2010). We next tested whether NPC proteins that are important for peripheral targeting for *GAL1-10* are required for clustering. Loss of the nuclear pore basket components Nup1, Nup60, and Mlp2 blocked targeting of *GAL1-10* locus to the nuclear periphery in galactose

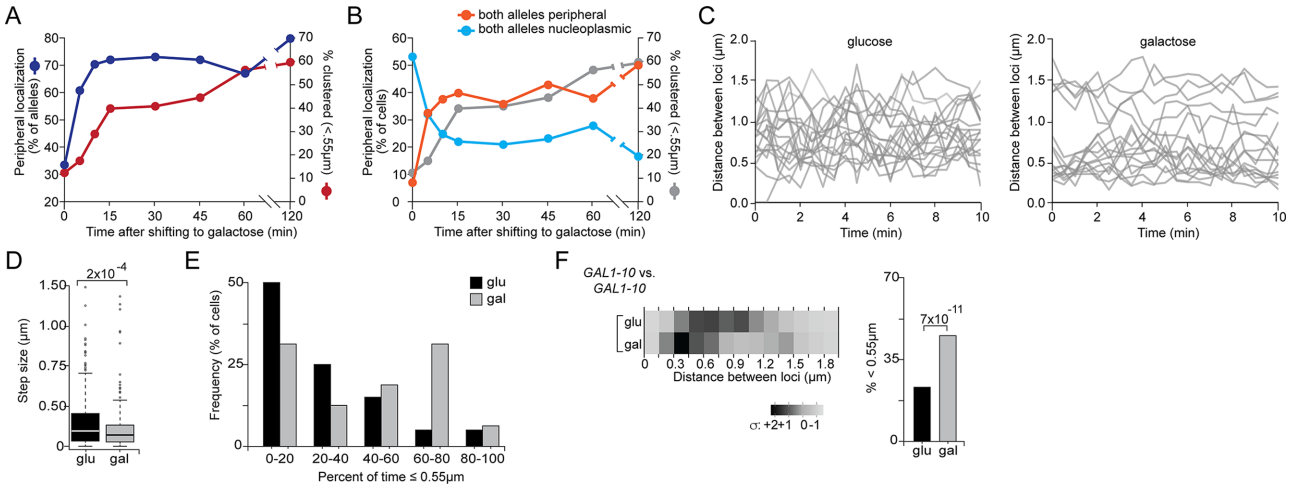

FIGURE 4: *GAL1-10* interchromosomal clustering dynamics. (A, B) Haploid cells with the LacO array integrated at the 3′ end of *GAL1* were shifted from glucose to galactose medium. An aliquot of cells was removed from the culture at the indicated times, and the peripheral localization of *GAL1-10* was scored (blue circles in A; orange/cyan in B). Each time point represents 30–50 cells. Diploid cells with both *GAL1-10* alleles marked with the LacO array were shifted from glucose to galactose medium and imaged at the indicated times. The distance between the two *GAL1-10* alleles was measured and is plotted as percentage of cells in which the two alleles were <0.55 µm apart (red circles in A; gray in B). Each data point is from 100 cells. (C) A population of diploid cells with both *GAL1-10* alleles labeled with the LacO array grown in glucose or galactose medium was imaged every 30 s for 10 min, and the distance between the *GAL1-10* alleles in each of 20 cells was measured. (D) Distribution of change in distance between the *GAL1-10* alleles between time points (i.e., step size) in the cells analyzed in C. The *p* value is from a Student's *t* test. (E) Data presented in C were analyzed to determine percentage of cells in which the *GAL1-10* alleles were <0.55 µm apart for the indicated fractions of the 20 time points of the 10-min experiment in either glucose or galactose. (F) Data from the cells monitored in C were pooled for each growth condition and the resulting distribution (left) and percentage clustering (right) plotted. The *p* values are from a Fisher exact test.

(Figure 5A). Although it was previously reported to be required for peripheral localization of *GAL1-10* (Dieppois *et al.*, 2006), we did not observe a defect in peripheral recruitment in a mutant lacking Mlp1, another NPC basket component (Figure 5A). However, *INO1* targeting to the nuclear periphery is also dependent on Mlp2 but not on Mlp1 (Ahmed *et al.*, 2010). Loss of Nup1, Nup60, and Mlp2 also disrupted clustering of *GAL1-10* alleles (Figure 5, B and C). These results suggest that interallelic clustering of *GAL1-10* alleles requires interaction with the nuclear pore.

Surprisingly, although Mlp1 is not required for *GAL1-10* targeting to the nuclear periphery, it is required for clustering of *GAL1-10* alleles (Figure 4C). In diploid strains homozygous for the *mlp1Δ* mutation, the mean distance between *GAL1-10* alleles was 0.91 ± 0.37 µm in glucose versus 0.83 ± 0.27 µm in galactose ($p = 0.38$; Wilcoxon rank sum test). Under both conditions, the *GAL1-10* alleles were within 0.55 µm in ≤20% of the cells (Figure 4C). Therefore Mlp1 plays an important role in promoting interchromosomal clustering but is not required for peripheral targeting. This suggests that these two phenomena have distinct molecular mechanisms.

GAL1-10 interchromosomal clustering requires active transcription

Active transcription is not required for *INO1* gene recruitment to the nuclear periphery (Brickner *et al.*, 2007). Similarly, *GAL1-10* repositioned to the nuclear periphery normally both in cells in which a temperature-sensitive allele of RNA polymerase II (*rpb1-1*; Nonet *et al.*, 1987) was inactivated and in cells treated with the transcriptional inhibitor 1,10-*o*-phenanthroline (OP) before cells were shifted to galactose (Figure 6A). Therefore, like *INO1*, active RNA polymerase II–mediated transcription is not required for *GAL1-10* targeting to the nuclear periphery.

In contrast, *GAL1-10* clustering was blocked when RNA polymerase II was inactivated or inhibited before cells were shifted to galactose (Figure 6B). At the permissive temperature, *GAL1-10* alleles clustered normally in *rpb1-1* cells (<0.55 µm, 45%; mean distance of 0.68 ± 0.35 µm; Figure 6Bb). However, at the restrictive temperature, *GAL1-10* clustering was blocked in *rpb1-1* cells (<0.55 µm, 17%,; mean distance of 0.94 ± 0.40 µm; Figure 6Bc). Similarly, addition of OP blocked clustering of *GAL1-10* alleles (<0.55 µm, dropped from 51% [mean distance of 0.65 ± 0.37 µm] to 20% [mean distance of 0.89 ± 0.37 µm]; Figure 6Bf). Therefore transcription is required to establish *GAL1-10* clusters.

To test whether transcription plays an important role in maintaining *GAL1-10* interchromosomal clustering after it is established, we inactivated RNAPII with OP 1 h after shifting to galactose. In this regime, the *GAL1-10* alleles remained clustered after inactivation of RNAPII (Figure 6Be). This suggests that active transcription is required to establish, but not maintain, *GAL1-10* interchromosomal clustering.

Gal4, a transcriptional activator that is essential for *GAL1-10* expression, is not required for peripheral localization of *GAL1-10*; in fact, mutants lacking Gal4 showed *constitutive* targeting of *GAL1-10* to the nuclear periphery (Figure 6A). This may reflect the fact that Gal80, which is able to block zip code function (Randise-Hinchliff *et al.*, 2016), is recruited to the *GAL1-10* promoter through interaction with Gal4 (Pilauri *et al.*, 2005). Thus Gal4 is involved in regulating zip code–mediated targeting to the periphery but is not required for peripheral localization. In contrast, loss of Gal4 led to a strong defect in clustering of *GAL1-10* alleles (Figure 6Cc). This suggests that transcription of the *GAL1-10* locus (or another Gal4-dependent *GAL* gene) is required to establish interchromosomal clustering.

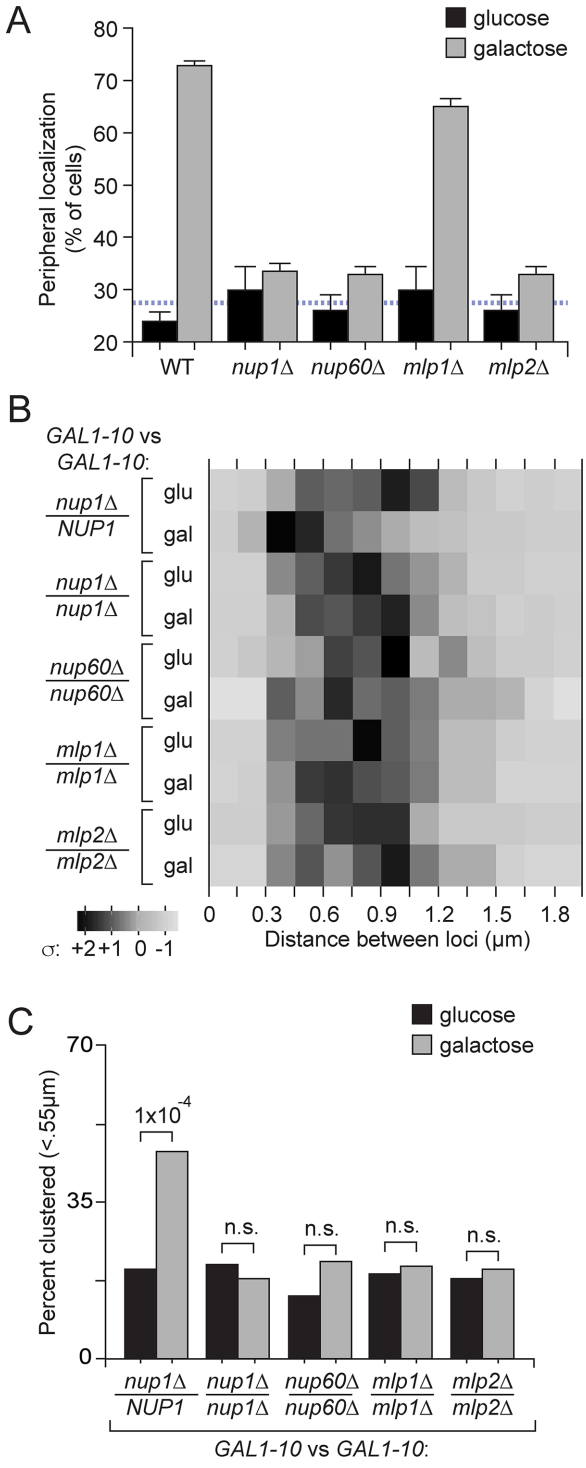

FIGURE 5: Peripheral targeting and interchromosomal clustering have distinct requirements for nuclear pore components.
(A) Wild-type or mutant cells were grown in glucose or galactose medium overnight, and the *GAL1-10* locus was scored for peripheral localization. Data presented are the average of three experiments of 30–50 cells each ± SEM. (B, C) Diploid cells of the indicated genotype were grown overnight in glucose or galactose medium. The distance between *GAL1-10* loci was measured, analyzed, and plotted as described in Figure 3. Note that a *nup1Δ/NUP1* heterozygote was used as a wild-type control, which gave results indistinguishable from those for the *NUP1/NUP1* diploid cells (e.g., Figure 3).

GAL1-10 positioning and interchromosomal clustering show coupled, out-of-phase cell cycle regulation

INO1, *GAL1*, and *HSP104* localization at the nuclear periphery is regulated through the cell cycle. These genes are positioned at the nuclear periphery during G1 and G2/M phase but briefly dissociate from the nuclear envelope during S phase (Brickner and Brickner, 2010, 2011). Clustering of *INO1* is maintained in the nucleoplasm during S phase (Brickner *et al.*, 2012). However, it is unclear whether clustering is also regulated through the cell cycle. To determine whether *GAL1-10* clustering is regulated through the cell cycle, we measured the distances between *GAL1-10* alleles in an asynchronous population grown in galactose and classified each cell as unbudded (G1 phase), small-budded (S phase), or large-budded (G2/M phase; Figure 7A). This analysis revealed that clustering of *GAL1-10* alleles was also disrupted through the cell cycle but not in phase with peripheral localization: *GAL1-10* alleles were clustered in G1 cells (55% with <0.55 μm; mean distance of 0.65 ± 0.35 μm) and largely remained clustered in S-phase cells (35% with <0.55 μm; mean distance of 0.74 ± 0.41 μm) but were not clustered in G2/M cells (4% with <0.55 μm; mean distance of 1.14 ± 0.35 μm; Figure 7, B and C). The observed clustering was specific; *URA3* did not cluster with *GAL1-10* at any point in the cell cycle and clustering required GRS4 and Gal4 (Figure 7, B and C). This suggests that in S phase, the *GAL1-10* alleles cluster in the nucleoplasm, whereas during G2/M, the *GAL1-10* alleles reposition to the nuclear periphery but do not cluster.

To confirm that *GAL1-10* clustering was maintained during S phase and lost during mitosis, we arrested cells during S phase by treatment with hydroxyurea and during mitosis by treatment with nocodazole. In S phase–arrested cells, *GAL1-10* alleles showed significant clustering (37% with <0.55 μm; Figure 7C). However, in cells arrested during mitosis using nocodazole, which induces the spindle checkpoint and prevents loss of cohesion between the products of DNA replication (Guacci *et al.*, 1997; Michaelis *et al.*, 1997), the two visible *GAL1-10* alleles were not clustered (16% with <0.55 μm; mean distance of 1.13 ± 0.52 μm; Figure 7C). Removing nocodazole and transferring the cells into fresh galactose medium led to rapid reestablishment of *GAL1-10* clustering during G1 (Figure 7D). Therefore the clustering of the *GAL1-10* alleles is regulated dynamically through the cell cycle. Furthermore, although both gene recruitment to the nuclear periphery and interchromosomal clustering are regulated through the cell cycle, their regulation is out of phase.

The changes in peripheral localization and clustering through the cell cycle are not correlated with significant changes in the mRNA level of *GAL1* or *GAL10* (Supplemental Figure S2), suggesting that they represent active regulation rather than indirect effects of changes in transcription. Our previous work implicated the phosphorylation of Nup1 in regulating peripheral targeting through the cell cycle (Brickner and Brickner, 2010). Nup1 is essential for *GAL1-10* targeting to the nuclear periphery and interchromosomal clustering. Phosphorylation of Nup1 by cyclin-dependent kinase (Cdk) at two sites (S161 and T344) is required for localization of active *INO1* and *GAL1-10* to the nuclear periphery (Brickner and Brickner, 2010). When both of the residues were mutated to cysteines to block phosphorylation, active *INO1* and *GAL1-10* no longer localized to the nuclear periphery. Conversely, in cells expressing phosphomimetic mutants (S161D or T344D), active *INO1* and *GAL1-10* are retained at the nuclear periphery through S phase (Brickner and Brickner, 2010). Thus phosphorylation of a critical nuclear pore protein during G1 and G2/M (and presumably dephosphorylation of these sites

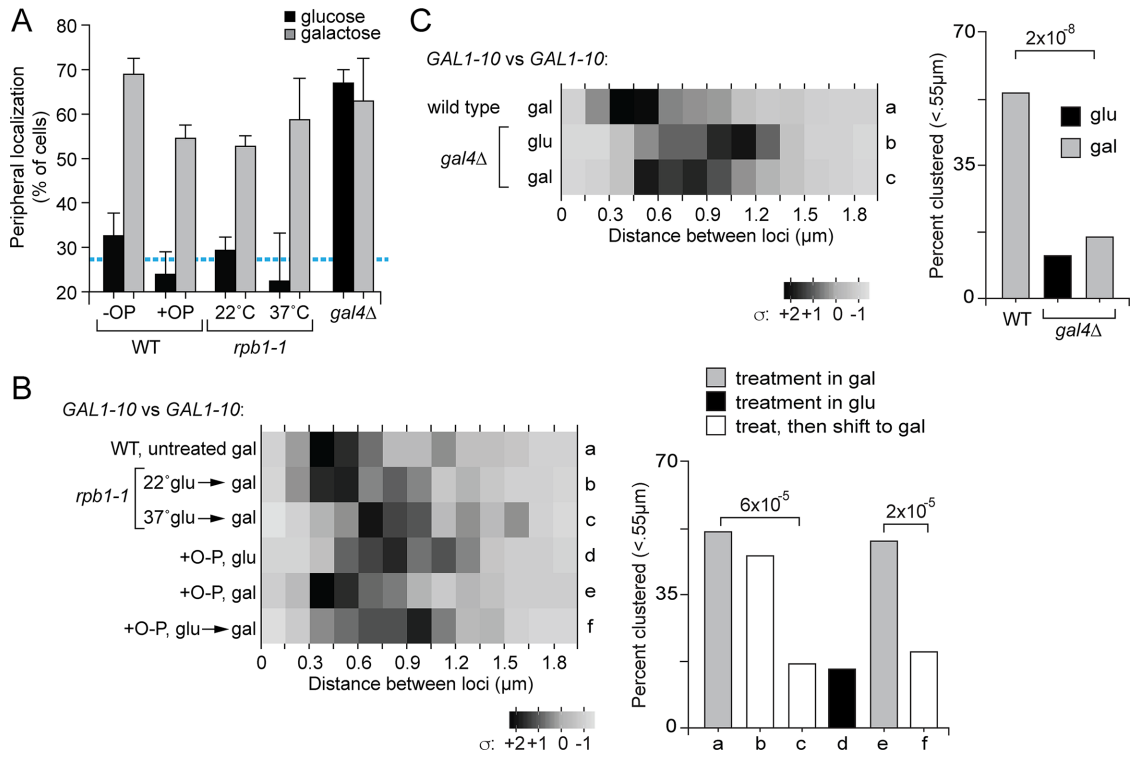

FIGURE 6: Establishment of *GAL1-10* interchromosomal gene clustering requires active transcription. (A) Haploid WT, *rpb1-1*, or *gal4*Δ cells were grown in glucose and galactose. The *rbp1-1* mutant was either maintained at the permissive temperature (22°C) or shifted to the restrictive temperature (37°C) for 30 min before being shifted to galactose at the same temperature. *GAL1-10* LacO was scored for peripheral localization. WT haploid cells were also grown in glucose ± 100 μg/ml OP for 20 min before induction in galactose ± OP. For each treatment, data represent the average of three separate experiments of 30–50 cells ± SEM. (B) Diploid WT or *rpb1-1* mutant cells with both alleles of *GAL1-10* marked with the LacO array were grown in glucose at either 22°C or shifted to 37°C for 30 min before being shifted to galactose at 22°C or 37°C, respectively. OP, 100 μg/ml, was added to WT cells either before (experiment f) or 1 h after (experiment e) switching to galactose. The distance between *GAL1-10* alleles was measured, analyzed, and plotted as described in Figure 2. (C) WT and *gal4*Δ mutant diploid cells were grown in glucose overnight or switched to galactose medium for 1 h. The distance between *GAL1-10* alleles was measured and plotted as in Figure 3.

during S phase) dynamically regulates the localization of inducible genes to the nuclear periphery through the cell cycle.

Nup1 is required for *GAL1-10* clustering (Figure 5). An ectopically expressed wild-type copy of *NUP1* complements the *nup1*Δ mutant phenotypes (temperature sensitivity, proper gene localization during gene activation (Brickner and Brickner, 2010), and interchromosomal clustering; Figure 5B). Phosphorylation of Nup1 is also required for interchromosomal clustering; Nup1 lacking the phosphorylation sites (ΔP) failed to complement the loss of *GAL1-10* clustering (Figure 7, E and F). Furthermore, Nup1 having one of the two sites replaced with a phosphomimetic aspartate (PM) restored *GAL1-10* clustering (Figure 7, E and F). Thus both peripheral recruitment and interchromosomal clustering of *GAL1-10* locus require Cdk phosphorylation of Nup1.

To test whether repositioning of *GAL1-10* clusters to the nucleoplasm during S phase is required for their separation during M phase, we asked whether the phosphomimetic mutant of Nup1, which maintains *GAL1-10* at the nuclear periphery throughout the cell cycle (Brickner and Brickner, 2010), could prevent the loss of *GAL1-10* clustering during G2/M. In wild-type cells arrested in M phase with nocodazole, *GAL1-10* alleles were unclustered (Figure 7, E and F), but in cells expressing Nup1-PM (T344D) arrested with nocodazole, *GAL1-10* alleles remained clustered (47% with <0.55 μm; mean distance of 0.66 ± 0.33 μm; Figure 7, E and F). These results suggest that the loss of *GAL1-10* clustering during M phase requires the repositioning of *GAL1-10* to the nucleoplasm during S phase and that both are controlled by the dephosphorylation of Nup1.

DISCUSSION

The position of *GAL1-10* within the nucleus is controlled by small, *cis*-acting DNA elements called GRS4 and GRS5. Both of these elements function as DNA zip codes: they are necessary and sufficient to confer targeting to the nuclear periphery. However, the GRS4 zip code can also promote interchromosomal clustering with loci having the same zip code. Thus this work supports the view that there are at least two different types of DNA elements that influence the spatial organization of the budding yeast genome: those that affect gene positioning only and those that also promote interchromosomal clustering.

Interchromosomal clustering of genes is a common phenomenon in biology. We found that targeting to the nuclear periphery through interaction with the NPC is often associated with interchromosomal clustering, both between alleles of the same gene and between heterologous loci that share certain zip codes (Brickner *et al.*, 2012, 2015; Randise-Hinchliff *et al.*, 2016). Computational modeling of Hi-C chromosome capture data suggested that the *GAL* genes cluster together (Gehlen *et al.*, 2012). Furthermore, chromosome conformation capture reveals an interallelic interaction

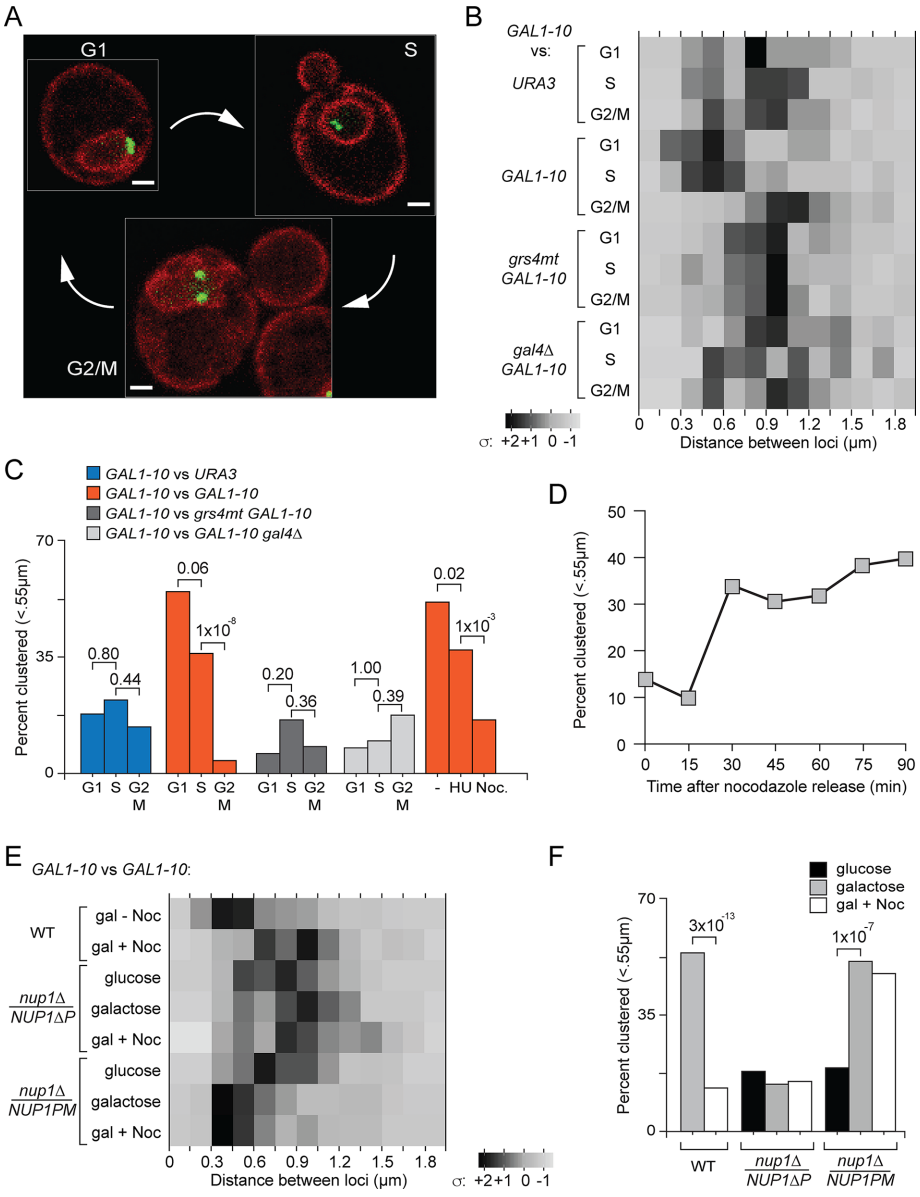

FIGURE 7: *GAL1-10* gene clustering is regulated through the cell cycle. (A) Representative confocal micrographs depicting cells at different cell cycle stages: Top left, unbudded cell (G1 phase); top right, small-budded cell (S phase); lower center, large-budded cell (G2/M phase). Scale bar, 1 μm. (B) Distribution of distances between *GAL1-10* alleles in an asynchronous population of wild-type cells grown overnight in galactose and scored according to bud morphology, plotted as in Figure 3. (C) Wild-type diploid cells were grown in galactose and incubated ± 100 mM hydroxyurea (HU) or 15 μg/ml nocodazole (Noc) for 2 h before imaging. The distance between loci was measured in 100 cells for each treatment, and the percentage of cells in which the two alleles are <0.55 μm apart is plotted. (D) Diploid cells with LacO arrays marking both alleles of *GAL1-10* were grown in galactose overnight, treated with nocodazole for 2 h, and released into galactose medium without the drug, and time points were taken every 15 min for 90 min. The percentage with <0.55 μm was plotted at each time point. (E, F) Wild-type cells and *nup1Δ/nup1-ΔP*, or *nup1Δ/NUP1-PM* mutants (see the text for details) were grown in galactose medium with or without nocodazole for 2 h. The distance between the *GAL1-10* alleles was measured and plotted as in Figure 3.

between two ectopic copies of the *GAL1-10* promoter, and this interaction correlates with transvection, or interallelic transcriptional regulation in-*trans* (Zhang and Bai, 2016). Consistent with these observations, we find that the *GAL1-10* alleles cluster together when active but not when repressed. Within the population, clustering leads to a clear and significant shift in both the distribution of distances between the alleles and the fluctuation of distances between the alleles. This is in contrast to a study in which the distance between the alleles of *GAL1-10* was monitored in glucose and galactose in live cells (Backlund *et al.*, 2014). Although that study reported a slight increase in the fraction of cells in which the two alleles were <0.55 μm in galactose, it did not observe a significant difference in the mean distance between the *GAL1-10* alleles. It is conceivable that there are technical reasons for this difference (e.g., using one type vs. two types of arrays, integration site of arrays, yeast strain background). However, our experiments not only observed the phenomenon of *GAL1-10* clustering, but they also identified genetic, cell biological, and chemical perturbations to disrupt it.

Targeting of *GAL1-10* to the nuclear periphery and *GAL1-10* clustering are not perfectly coupled. The present study identified six ways in which the two phenomena can be mechanistically distinguished:

1. Kinetics of targeting versus clustering. *GAL1-10* repositions to the nuclear periphery very rapidly, but the clustering of *GAL1-10* occurred over a much longer time scale.
2. DNA zip codes. Whereas either GRS4 or GRS5 is sufficient to cause targeting to the nuclear periphery, GRS4 alone controls clustering.
3. Requirement for transcription. Targeting to the nuclear periphery occurs normally in the absence of transcription, but clustering does not.
4. Requirement for Gal4. Targeting to the nuclear periphery occurs normally in the absence of Gal4, but clustering does not.
5. Requirement for Mlp1. Targeting to the nuclear periphery occurs normally in the absence of Mlp1, but clustering does not.
6. Cell cycle regulation. Whereas peripheral localization is lost during S phase and re-established during G2/M, clustering persists during S phase and lost during G2/M.

Together these results suggest that targeting to the nuclear periphery and interchromosomal clustering are mechanistically overlapping but distinct phenomena.

Targeting to the nuclear pore complex is a prerequisite for *GAL1-10* clustering; loss of nuclear pore proteins essential for peripheral localization blocks clustering. However, targeting to the nuclear periphery is not sufficient per se to promote interchromosomal clustering, and clustering can be maintained in the nucleoplasm during S phase, away from the NPC. Finally,

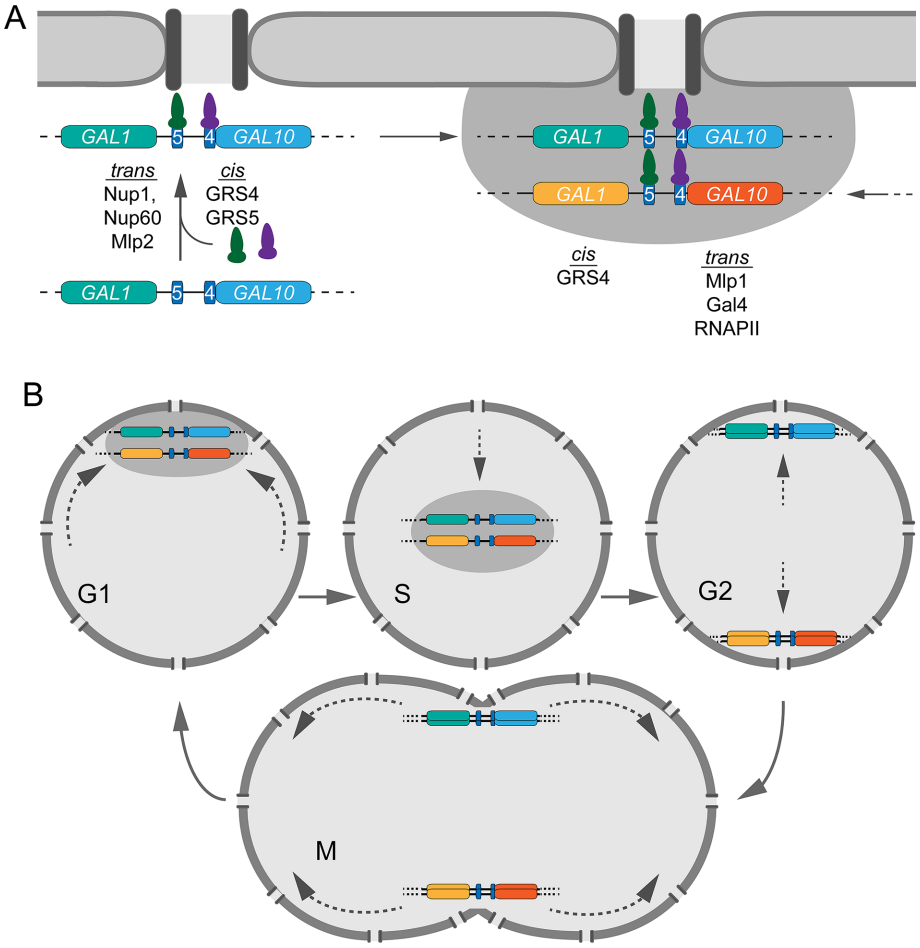

FIGURE 8: Model for zip code–mediated gene recruitment and interchromosomal clustering of the *GAL1-10* locus. (A) Schematic representation of gene recruitment and possible mechanism for gene clustering. Two alleles of *GAL1-10* are shown in blue and orange. Both *cis* and *trans* factors required for peripheral targeting and interchromosomal clustering are highlighted. (B) Clustering of *GAL1-10* alleles through the cell cycle. During G1, the two alleles of *GAL1-10* are clustered at the nuclear periphery. On the initiation of DNA replication during S phase, the two alleles remain clustered in the nucleoplasm. During G2, the (duplicated) alleles of *GAL1-10* are unclustered at the nuclear periphery, and during mitosis, segregation of the alleles to the mother and the daughter precedes the reestablishment of clustering during G1.

whereas all proteins that are required for peripheral localization are required for clustering, several factors not required for peripheral targeting are required for clustering (Figure 8A). Similarly, blocking RNA polymerase II activity globally or preventing *GAL1-10* transcription had no effect on the targeting of *GAL1-10* to the periphery but prevented clustering. However, once clusters were formed, they were not disrupted by inactivation of RNA polymerase II. Thus interaction with the NPC and transcription play essential roles in the establishment but not the maintenance of clustering.

Our results lead us to speculate that nuclear pore proteins and/or RNA may provide the physical basis of interchromosomal clustering. The requirement for transcription to establish clustering raises the possibility that RNA and RNA-binding proteins are involved. Such multivalent ribonucleoproteins play critical roles in the formation of nuclear "bodies," which behave as phase-separated droplets (Kaiser *et al.*, 2008; Brangwynne *et al.*, 2009, 2011; Shevtsov and Dundr, 2011; Kato *et al.*, 2012; Berry *et al.*, 2015; Zhang *et al.*, 2015; Zhu and Brangwynne, 2015). Nuclear pore proteins, through their multivalent, natively unstructured domains, could interact with transcription factors, RNA transport factors, and RNA to facilitate the formation of such compartments, stabilizing interchromosomal interactions. Such a "compartment" might concentrate certain proteins, affecting transcription or mRNA metabolism. Phase-separated protein droplets dynamically form and dissociate in response to small changes in the concentrations of protein and ligand (Li *et al.*, 2012; Weber and Brangwynne, 2015), and so their association with nuclear pore proteins would provide a mechanism to readily assemble and disassemble interchromosomal clusters.

Targeting to the NPC leads to interchromosomal associations that are stabilized by a transcription- and Mlp1-dependent mechanism (Figure 8A). The NPC may either provide a platform that enhances the efficiency of homotypic interactions between genes with the same zip code or play a more active role in facilitating clustering. Mlp1 promotes the looping of the 5′ and 3′ ends of the *GAL1-10* gene (Tan-Wong *et al.*, 2009), suggesting that Mlp1 may have a more general role as an architectural regulator of both *cis* and *trans* chromatin interactions. The metazoan homologue of Mlp1, TPR, extends away from the NPC into the nucleoplasm (Fontoura *et al.*, 2001). Therefore this conserved filamentous protein could provide a structural element that facilitates the interaction between chromosomes in other eukaryotes.

The cell cycle regulation of peripheral targeting and interchromosomal clustering are interdependent but out of phase (Figure 8B). Whereas peripheral localization of *GAL1-10* (and other genes; Brickner and Brickner, 2010, 2011) is lost during S phase, *GAL1-10* clustering is maintained through S phase but lost during G2/M. Consistent with this observation, in an asynchronous population, we observed two distinct types of cells: those in which the genes are clustered, and those in which they are not. A mutation in the nuclear pore protein Nup1 that mimics constitutive phosphorylation at a critical Cdk site causes *GAL1-10* to remain at the nuclear periphery through S phase and also maintains clustering through G2/M. Therefore the loss of clustering during G2/M requires the loss of peripheral localization during S phase. In other words, these two events are separately regulated by a common connection to Cdk phosphorylation of a nuclear pore protein. Because the molecular requirements for clustering are distinct from those of peripheral localization, it is plausible that loss of peripheral localization is an initiating event that is necessary for a subsequent event that disrupts clustering and is coordinated with the cell cycle.

Gene positioning has been proposed to facilitate the spatial and functional compartmentalization of the genome. The subnuclear positioning of the *GAL1-10* locus provides an excellent model for this notion. The positioning of *GAL1-10* within the nucleus and its positioning with respect to other genes in the genome are controlled by two interdependent, mechanistically distinct phenomena: targeting to the nuclear pore complex and interchromosomal clustering.

MATERIALS AND METHODS

Chemicals, media, and growth conditions

All chemicals used in this study were purchased from Sigma-Aldrich (St. Louis, MO). All restriction enzymes and modifying enzymes were purchased from New England Biolabs (Ipswich, MA). All yeast media components were purchased from Sunrise Science Products (San Diego, CA) and prepared as described (Burke *et al.*, 2000).

Yeast strains, plasmids, and molecular biology

Yeast strains used in this study are listed in Supplemental Table S1. Plasmids pAFS144 (Straight *et al.*, 1996), p5LacIGFP, pER04 (Randise-Hinchliff *et al.*, 2016), pZIP Kan (Egecioglu and Brickner, 2011), p6LacO128-GAL1 (Brickner *et al.*, 2007), pFA6a-His3MX6, and pFA6a-kanMX6 (Longtine *et al.*, 1998) have been described. The 667–base pair *GAL1-10* promoter was PCR-amplified TOPO cloned to create pCR2.1-GAL1-10pro. This plasmid was subjected to QuikChange mutagenesis to generate pCR2.1-GAL1-10pro grs4mt, pCR2.1-GAL1-10pro grs5mt, and pCR2.1-GAL1-10pro grs4,5mt. Plasmid p6LacO128-GAL1-10prom was made by insertion of the *GAL1-10* promoter from pCR2.1-GAL1-10pro into p6LacO128 (Brickner and Walter, 2004).

Strains used to test the zip code activity of DNA sequences were generated using the integration cassette in the plasmid pZipKan described by Egecioglu *et al.* (2014). Briefly, the plasmid bears a cassette with a *Kan*^{r} gene flanked by sequences homologous to p6LacO128 and a *Pac*I site into which candidate DNA sequences of >10 base pairs were cloned (Figure 1B, top). Fragments of ≤10 base pairs were synthesized as part of the primers used for amplification. The cassette was either digested with *Kpn*I plus *Eco*RV (for cloned fragments) or amplified by PCR (for those synthesized as part of the primer) and transformed into a yeast strain in which p6LacO128 was integrated at *URA3* (Figure 1B, top). Insertion of the cassette conferred G418 resistance and was confirmed by sequencing PCR products from the genomic DNA from the candidates. Knockout mutant yeast strains were generated using PCR amplification of deletion cassettes and homologous recombination (Longtine *et al.*, 1998). To create mutations in the chromosomal *GAL1-10* promoter, the promoter was first replaced with a double-selection cassette made as follows. The *URA3* gene was PCR amplified from pRS306 (base pairs 123–1321; Sikorski and Hieter, 1989), and *Sac*I and *Bam*HI sites were appended to the 5′ and 3′ ends, respectively. *URA3* was cloned into pBluescript SK+ as a *Sac*I–*Bam*HI fragment to generate pBS-URA3. The *SUP4-o* mutant allele was cloned by PCR amplification from the genomic DNA of a *SUP4-o* yeast strain, and the *Kpn*I and *Xho*I sites were appended to the 5′ and 3′ ends of the PCR product. This PCR product was cloned as a *Kpn*I–*Xho*I fragment into pBS-URA3 to generate pBS-URA-SUP in which the *URA3* and *SUP4-o* were arranged tail to tail. The *URA-SUP* was amplified using the primers 5′-TTATATTGAATTTTCAAAAATTCTTACTTTTTTTTTGGATGGACGCAAAGAAGGCGGGTGTCGGGGCTG-3′ and 5′-TTTTCGGCCAATGGTCTTGGTAATTCCTTTGCGCTAGAATTGAACTCAGGGACCGGATAATTATTTGAAATCTCTTTTTC-3′ from pBS-URA-SUP for integration at *GAL1-10*. Replacement of the *GAL1-10* promoter with *URA3-SUP4-o* was selected on –Ura –Ade plates; *URA3* complements the *ura3-1* mutation, and *SUP4-o* suppresses the *ade2-1* ochre mutation. Transformants were Gal$^-$, and the structure of the integration was confirmed using PCR from genomic DNA. The resulting strain is sensitive to 5-fluoroorotate (5-FOA) because it is Ura$^+$ and canavanine because *SUP4-o* also suppresses the *can1-100* mutation. Therefore, to select for reintroduction of wild-type or mutant versions of the *GAL1-10* promoter upon transformation with PCR products extending beyond the boundaries of the promoter, in a second step, FOA^R Can^R transformants were selected after growth overnight on yeast extract/peptone/dextrose and then screened for Ade$^-$. The reintroduced promoters were confirmed by PCR and sequenced to verify mutations. The *SUP-o* suppression of *ade2-1* in the first step led to a change in colony morphology from pink to white, and replacement of the cassette in the second step restored the pink colony morphology. All of the pink colonies tested had replaced the *URA3-SUP4-o* cassette with the *GAL1-10* promoter. Site-directed mutagenesis was performed with Pfu polymerase and mutagenic primers detailed in Supplemental Table S2. Strains with two copies of *GAL1-10* tagged with the LacO array were made by mating *MAT***a** and *MAT*α cells with complementary auxotrophies and selecting for prototrophic diploids.

Cultures were grown in minimal medium with 2% glucose or 2% galactose at 30°C with constant shaking before being harvested for experiments. Unless noted, cultures were grown overnight before imaging. The temperature-sensitive *rpb1-1* strain was grown at the permissive temperature of 22°C before being shifted for 30 min to the restrictive temperature of 37°C. Cells were harvested and washed into galactose medium prewarmed to 37°C and incubated for 1 h before imaging.

Confocal microscopy and simulation

Cultures were grown as described, and 1 µl was spotted onto a microscope slide and visualized on a Leica SP5 as described (Egecioglu *et al.*, 2014). *Z*-stacks of ≥5 µm, comprising the whole yeast cell, were collected. For experiments in which we scored peripheral localization, ≥30–50 cells were scored per biological replicate and at least three biological replicates were scored for each average. Cells scored for peripheral localization met the following criteria: 1) the strain only had one visible dot, and 2) the dot was in the middle one-third of the nucleus. Similarly, for experiments in which we measured the distance between two loci, we only analyzed cells with 1) two visible dots and 2) in which both dots were in the same or an adjacent *z*-slice. Cells were excluded if they had abnormal nuclear morphology, only a single dot, or more than two dots. Confocal images were merged and quantified, and distances were measured using LAS AF software.

The simulation of the position of two genes within a nucleus of 1-µm radius was produced by randomly generating two points, each with *x*, *y*, and *z* values between 1 and –1 µm and with total distance from origin ≤1 µm. The script is given in the Supplemental Materials. Three unbiased simulations of 1000 nuclei generated an average distance between two genes of 1.03 µm, in agreement with the expected value of 36/35, with 10.7% with <0.55 µm. To simulate our method of *z*-stack image acquisition, in which we only score cells in which the two spots are 1) in the same or adjacent slices and 2) resolvable from each other, nuclei in which either the *z*-coordinates of the two genes was >0.64 µm or the *x*, *y*-distance was <0.15 µm were discarded. This filtered set of nuclei produced 2928 nuclei, which were used to generate the distribution in Figure 3.

Data analysis

For clustering experiments, distances for ≥100 cells were measured. The distances to be compared were organized into columns in a comma-separated text file and input into an R script, which binned data, calculated SDs for each bin, and generated the heat map display (Markdown file in the Supplemental Materials). Statistical tests performed using R were the Wilcoxon rank sum test for comparison between two distributions and the Fisher exact test for comparisons for fraction of the population with <0.55 µm.

Single-molecule FISH

Single-molecule FISH was performed as described (Rahman and Zenklusen, 2013) with the following modifications. *GAL1* probes were designed using the Stellaris Probe Designer (LGC Biosearch Technologies, Novato, CA). The 48 × 20 base oligonucleotides targeting the *GAL1* open reading frame (ORF; Supplemental Table S3) were synthesized and conjugated with the fluorophore Quasar 570 (LGC Biosearch Technologies). Yeast strains were grown overnight at 25°C in SDC complete glucose medium. Cells were harvested at OD_{600} = 0.4 and switched to SC galactose medium for 2.5 h. Cells were fixed by adding paraformaldehyde (32% solution, EM grade; 15714; Electron Microscopy Science, Hatfield, PA) to a final concentration of 4% at room temperature for 45 min. Cells were then washed three times with buffer B (1.2 M sorbitol and 100 mM potassium phosphate buffer, pH 7.5) and resuspended in 500 µl of spheroplast buffer (buffer B containing 20 mM VRC [ribonucleoside–vanadyl complex; S1402S, New England Biolabs] and 25 U of lyticase enzyme (L2524; Sigma-Aldrich]) per OD of cells for ~10 min at 30°C. Digested cells were washed once with buffer B and resuspended in 1 ml of buffer B. A 150-µl amount of cells was seeded on 18-mm polylysine-treated coverslips and incubated at 4°C for 30 min. Coverslips were washed once with buffer B, gently covered with ice-cold 70% ethanol, and stored at –20°C.

For hybridization, coverslips were rehydrated by adding 2× saline–sodium citrate (SSC) at room temperature twice for 5 min. Coverslips were prehybridized with a mix containing 10% formamide (205821000; ACROS Organics)/2× SSC at room temperature for 30 min. For each coverslip, the *GAL1* probe mix (sufficient to obtain a final concentration in the hybridization mix of 125 nM) was added to 5 µl of 10 mg/µl *Escherichia coli* tRNA/single-stranded DNA (1:1) mix and dried with a SpeedVac. The dried mixture was resuspended in 25 µl of hybridization mix (10% formamide, 2× SSC, 1 mg/ml bovine serum albumin, 10 mM VRC, 5 mM $NaHPO_4$, pH 7.5), heated at 95°C for 3 min, and then hybridized at 37°C for 3 h in the dark. On hybridization, coverslips were washed twice with prehybridization mix for 30 min at 37°C, once with 0.1% Triton X-100 in 2× SSC for 10 min at room temperature, and once with 1× SSC for 10 min at room temperature. Nuclei were stained with 0.5 µg/ml 4′,6-diamidino-2-phenylindole (DAP) in 1× PBS for 2 min at room temperature and washed with 1× PBS for 10 min at room temperature. Coverslips were mounted on glass slides using ProLong Gold antifade (Thermo Fisher, Skokie, IL). Images were acquired using an Olympus BX61 wide-field epifluorescence microscope with a 100×/1.35 numerical aperture UPlanApo objective. Samples were visualized using an X-Cite 120 PC lamp (EXFO) and an ORCA-R2 digital charge-coupled device camera (Hamamatsu, Hamamatsu City, Japan). MetaMorph software (Molecular Devices, Sunnyvale, CA) was used for acquisition. *Z*-sections were acquired at 200-nm intervals over an optical range of 8.0 µm. Image pixel size was *xy*, 64.5 nm. FISH images were analyzed using FISH Quant (Mueller *et al.*, 2013). Briefly, after background subtraction, the FISH spots in the cytoplasm were fit to a three-dimensional (3D) Gaussian to determine the coordinates of the mRNAs. The intensity and width of the 3D Gaussian were thresholded to exclude nonspecific signal. The average intensity of all the mRNAs was used to determine the intensity of each transcription site.

ACKNOWLEDGMENTS

We thank members of the Brickner laboratory for helpful comments and suggestions on the manuscript and Erik Andersen for help with coding in R. This work was funded in part by the Chicago Biomedical Consortium with support from the Searle Funds at the Chicago Community Trust and by National Institutes of Health Grants R01 GM080484 (J.H.B.) and R01 GM057071 (R.H.S.), Swiss National Science Foundation (FNSNF) Fellowships P2GEP3_155692 and P300PA_164717 (E.T.), a predoctoral fellowship from the American Heart Association (V.S.), and an Undergraduate Research Grant from Northwestern University (K.V.). J.H.B. is the Loretta and Henry Shapiro Research Professor in Molecular Biology.

REFERENCES

Ahmed S, Brickner DG, Light WH, Cajigas I, McDonough M, Froyshteter AB, Volpe T, Brickner JH (2010). DNA zip codes control an ancient mechanism for gene targeting to the nuclear periphery. Nat Cell Biol 12, 111–118.

Backlund MP, Joyner R, Weis K, Moerner WE (2014). Correlations of three-dimensional motion of chromosomal loci in yeast revealed by the double-helix point spread function microscope. Mol Biol Cell 25, 3619–3629.

Berry J, Weber SC, Vaidya N, Haataja M, Brangwynne CP (2015). RNA transcription modulates phase transition-driven nuclear body assembly. Proc Natl Acad Sci USA 112, E5237–E5245.

Bian Q, Khanna N, Alvikas J, Belmont AS (2013). beta-Globin cis-elements determine differential nuclear targeting through epigenetic modifications. J Cell Biol 203, 767–783.

Brangwynne CP, Eckmann CR, Courson DS, Rybarska A, Hoege C, Gharakhani J, Julicher F, Hyman AA (2009). Germline P granules are liquid droplets that localize by controlled dissolution/condensation. Science 324, 1729–1732.

Brangwynne CP, Mitchison TJ, Hyman AA (2011). Active liquid-like behavior of nucleoli determines their size and shape in Xenopus laevis oocytes. Proc Natl Acad Sci USA 108, 4334–4339.

Brickner DG, Ahmed S, Meldi L, Thompson A, Light W, Young M, Hickman TL, Chu F, Fabre E, Brickner JH (2012). Transcription factor binding to a DNA zip code controls interchromosomal clustering at the nuclear periphery. Dev Cell 22, 1234–1246.

Brickner DG, Brickner JH (2010). Cdk phosphorylation of a nucleoporin controls localization of active genes through the cell cycle. Mol Biol Cell 21, 3421–3432.

Brickner DG, Brickner JH (2011). Gene positioning is regulated by phosphorylation of the nuclear pore complex by Cdk1. Cell Cycle 10, 392–395.

Brickner DG, Cajigas I, Fondufe-Mittendorf Y, Ahmed S, Lee PC, Widom J, Brickner JH (2007). H2A.Z-mediated localization of genes at the nuclear periphery confers epigenetic memory of previous transcriptional state. PLoS Biol 5, e81.

Brickner DG, Coukos R, Brickner JH (2015). Transcriptional memory leads to DNA zip code-dependent interchromosomal clustering. Microb Cell 2, 481–490.

Brickner JH, Walter P (2004). Gene recruitment of the activated INO1 locus to the nuclear membrane. PLoS Biol 2, e342.

Brown CR, Kennedy CJ, Delmar VA, Forbes DJ, Silver PA (2008). Global histone acetylation induces functional genomic reorganization at mammalian nuclear pore complexes. Genes Dev 22, 627–639.

Brown JM, Leach J, Reittie JE, Atzberger A, Lee-Prudhoe J, Wood WG, Higgs DR, Iborra FJ, Buckle VJ (2006). Coregulated human globin genes are frequently in spatial proximity when active. J Cell Biol 172, 177–187.

Burke D, Dawson D, Stearns T (2000). Methods in Yeast Genetics, Cold Spring Harbor, NY: Cold Spring Harbor Laboratory Press.

Cabal GG, Genovesio A, Rodriguez-Navarro S, Zimmer C, Gadal O, Lesne A, Buc H, Feuerbach-Fournier F, Olivo-Marin JC, Hurt EC, Nehrbass U (2006). SAGA interacting factors confine sub-diffusion of transcribed genes to the nuclear envelope. Nature 441, 770–773.

Capelson M, Liang Y, Schulte R, Mair W, Wagner U, Hetzer MW (2010). Chromatin-bound nuclear pore components regulate gene expression in higher eukaryotes. Cell 140, 372–383.

Casolari JM, Brown CR, Drubin DA, Rando OJ, Silver PA (2005). Developmentally induced changes in transcriptional program alter spatial organization across chromosomes. Genes Dev 19, 1188–1198.

Casolari JM, Brown CR, Komili S, West J, Hieronymus H, Silver PA (2004). Genome-wide localization of the nuclear transport machinery couples transcriptional status and nuclear organization. Cell 117, 427–439.

Cheutin T, Cavalli G (2012). Progressive polycomb assembly on H3K27me3 compartments generates polycomb bodies with developmentally regulated motion. PLoS Genet 8, e1002465.

Cremer T, Cremer M, Dietzel S, Muller S, Solovei I, Fakan S (2006). Chromosome territories–a functional nuclear landscape. Curr Opin Cell Biol 18, 307–316.

Dieppois G, Iglesias N, Stutz F (2006). Cotranscriptional recruitment to the mRNA export receptor Mex67p contributes to nuclear pore anchoring of activated genes. Mol Cell Biol 26, 7858–7870.

Dixon JR, Selvaraj S, Yue F, Kim A, Li Y, Shen Y, Hu M, Liu JS, Ren B (2012). Topological domains in mammalian genomes identified by analysis of chromatin interactions. Nature 485, 376–380.

Egecioglu D, Brickner JH (2011). Gene positioning and expression. Curr Opin Cell Biol 23, 338–345.
Egecioglu DE, D'Urso A, Brickner DG, Light WH, Brickner JH (2014). Approaches to studying subnuclear organization and gene-nuclear pore interactions. Methods Cell Biol 122, 463–485.
Fontoura BM, Dales S, Blobel G, Zhong H (2001). The nucleoporin Nup98 associates with the intranuclear filamentous protein network of TPR. Proc Natl Acad Sci USA 98, 3208–3213.
Gehlen LR, Gruenert G, Jones MB, Rodley CD, Langowski J, O'Sullivan JM (2012). Chromosome positioning and the clustering of functionally related loci in yeast is driven by chromosomal interactions. Nucleus 3, 370–383.
Gonzalez-Sandoval A, Towbin BD, Kalck V, Cabianca DS, Gaidatzis D, Hauer MH, Geng L, Wang L, Yang T, Wang X, *et al*. (2015). Perinuclear anchoring of H3K9-methylated chromatin stabilizes induced cell fate in C. elegans embryos. Cell 163, 1333–1347.
Guacci V, Koshland D, Strunnikov A (1997). A direct link between sister chromatid cohesion and chromosome condensation revealed through the analysis of MCD1 in S. cerevisiae. Cell 91, 47–57.
Guelen L, Pagie L, Brasset E, Meuleman W, Faza MB, Talhout W, Eussen BH, de Klein A, Wessels L, de Laat W, van Steensel B (2008). Domain organization of human chromosomes revealed by mapping of nuclear lamina interactions. Nature 453, 948–951.
Haeusler RA, Pratt-Hyatt M, Good PD, Gipson TA, Engelke DR (2008). Clustering of yeast tRNA genes is mediated by specific association of condensin with tRNA gene transcription complexes. Genes Dev 22, 2204–2214.
Harr JC, Luperchio TR, Wong X, Cohen E, Wheelan SJ, Reddy KL (2015). Directed targeting of chromatin to the nuclear lamina is mediated by chromatin state and A-type lamins. J Cell Biol 208, 33–52.
Jin F, Li Y, Dixon JR, Selvaraj S, Ye Z, Lee AY, Yen CA, Schmitt AD, Espinoza CA, Ren B (2013). A high-resolution map of the three-dimensional chromatin interactome in human cells. Nature 503, 290–294.
Kaiser TE, Intine RV, Dundr M (2008). De novo formation of a subnuclear body. Science 322, 1713–1717.
Kalverda B, Pickersgill H, Shloma VV, Fornerod M (2010). Nucleoporins directly stimulate expression of developmental and cell-cycle genes inside the nucleoplasm. Cell 140, 360–371.
Kato M, Han TW, Xie S, Shi K, Du X, Wu LC, Mirzaei H, Goldsmith EJ, Longgood J, Pei J, *et al*. (2012). Cell-free formation of RNA granules: low complexity sequence domains form dynamic fibers within hydrogels. Cell 149, 753–767.
Kind J, Pagie L, Ortabozkoyun H, Boyle S, de Vries SS, Janssen H, Amendola M, Nolen LD, Bickmore WA, van Steensel B (2013). Single-cell dynamics of genome-nuclear lamina interactions. Cell 153, 178–192.
Lemaitre C, Bickmore WA (2015). Chromatin at the nuclear periphery and the regulation of genome functions. Histochem Cell Biol 144, 111–122.
Leshner M, Devine M, Roloff GW, True LD, Misteli T, Meaburn KJ (2016). Locus-specific gene repositioning in prostate cancer. Mol Biol Cell 27, 236–246.
Li P, Banjade S, Cheng HC, Kim S, Chen B, Guo L, Llaguno M, Hollingsworth JV, King DS, Banani SF, *et al*. (2012). Phase transitions in the assembly of multivalent signalling proteins. Nature 483, 336–340.
Liang Y, Franks TM, Marchetto MC, Gage FH, Hetzer MW (2013). Dynamic association of NUP98 with the human genome. PLoS Genet 9, e1003308.
Light WH, Brickner DG, Brand VR, Brickner JH (2010). Interaction of a DNA zip code with the nuclear pore complex promotes H2A.Z incorporation and INO1 transcriptional memory. Mol Cell 40, 112–125.
Light W, Freaney J, Sood V, Thompson A, D'Urso A, Horvath C, Brickner JH (2013). A conserved role for human Nup98 in altering chromatin structure and promoting epigenetic transcriptional memory. PLoS Biol 11, e1001524.
Longtine MS, McKenzie A 3rd, Demarini DJ, Shah NG, Wach A, Brachat A, Philippsen P, Pringle JR (1998). Additional modules for versatile and economical PCR-based gene deletion and modification in Saccharomyces cerevisiae. Yeast 14, 953–961.
Luperchio TR, Wong X, Reddy KL (2014). Genome regulation at the peripheral zone: lamina associated domains in development and disease. Curr Opin Genet Dev 25, 50–61.
Meaburn KJ, Agunloye O, Devine M, Leshner M, Roloff GW, True LD, Misteli T (2016). Tissue-of-origin-specific gene repositioning in breast and prostate cancer. Histochem Cell Biol 145, 433–446.
Meaburn KJ, Gudla PR, Khan S, Lockett SJ, Misteli T (2009). Disease-specific gene repositioning in breast cancer. J Cell Biol 187, 801–812.
Meldi L, Brickner JH (2011). Compartmentalization of the nucleus. Trends Cell Biol 21, 701–708.
Michaelis C, Ciosk R, Nasmyth K (1997). Cohesins: chromosomal proteins that prevent premature separation of sister chromatids. Cell 91, 35–45.
Mueller F, Senecal A, Tantale K, Marie-Nelly H, Ly N, Collin O, Basyuk E, Bertrand E, Darzacq X, Zimmer C (2013). FISH-quant: automatic counting of transcripts in 3D FISH images. Nat Methods 10, 277–278.
Nonet M, Scafe C, Sexton J, Young R (1987). Eucaryotic RNA polymerase conditional mutant that rapidly ceases mRNA synthesis. Mol Cell Biol 7, 1602–1611.
Nora EP, Lajoie BR, Schulz EG, Giorgetti L, Okamoto I, Servant N, Piolot T, van Berkum NL, Meisig J, Sedat J, *et al*. (2012). Spatial partitioning of the regulatory landscape of the X-inactivation centre. Nature 485, 381–385.
Parada LA, McQueen PG, Munson PJ, Misteli T (2002). Conservation of relative chromosome positioning in normal and cancer cells. Curr Biol 12, 1692–1697.
Phillips-Cremins JE, Sauria ME, Sanyal A, Gerasimova TI, Lajoie BR, Bell JS, Ong CT, Hookway TA, Guo C, Sun Y, *et al*. (2013). Architectural protein subclasses shape 3D organization of genomes during lineage commitment. Cell 153, 1281–1295.
Pilauri V, Bewley M, Diep C, Hopper J (2005). Gal80 dimerization and the yeast GAL gene switch. Genetics 169, 1903–1914.
Pombo A, Jones E, Iborra FJ, Kimura H, Sugaya K, Cook PR, Jackson DA (2000). Specialized transcription factories within mammalian nuclei. Crit Rev Eukaryot Gene Expr 10, 21–29.
Ragoczy T, Bender MA, Telling A, Byron R, Groudine M (2006). The locus control region is required for association of the murine beta-globin locus with engaged transcription factories during erythroid maturation. Genes Dev 20, 1447–1457.
Rahman S, Zenklusen D (2013). Single-molecule resolution fluorescent in situ hybridization (smFISH) in the yeast S. cerevisiae. Methods Mol Biol 1042, 33–46.
Randise-Hinchliff C, Coukos R, Sood V, Sumner MC, Zdraljevic S, Meldi Sholl L, Brickner DG, Ahmed S, Watchmaker L, Brickner JH (2016). Strategies to regulate transcription factor-mediated gene positioning and interchromosomal clustering at the nuclear periphery. J Cell Biol 212, 633–646.
Rao SS, Huntley MH, Durand NC, Stamenova EK, Bochkov ID, Robinson JT, Sanborn AL, Machol I, Omer AD, Lander ES, Aiden EL (2014). A 3D map of the human genome at kilobase resolution reveals principles of chromatin looping. Cell 159, 1665–1680.
Rodley CD, Pai DA, Mills TA, Engelke DR, O'Sullivan JM (2011). tRNA gene identity affects nuclear positioning. PLoS One 6, e29267.
Rohner S, Kalck V, Wang X, Ikegami K, Lieb JD, Gasser SM, Meister P (2013). Promoter- and RNA polymerase II-dependent hsp-16 gene association with nuclear pores in Caenorhabditis elegans. J Cell Biol 200, 589–604.
Schneider M, Hellerschmied D, Schubert T, Amlacher S, Vinayachandran V, Reja R, Pugh BF, Clausen T, Kohler A (2015). The nuclear pore-associated TREX-2 complex employs mediator to regulate gene expression. Cell 162, 1016–1028.
Schoenfelder S, Sexton T, Chakalova L, Cope NF, Horton A, Andrews S, Kurukuti S, Mitchell JA, Umlauf D, Dimitrova DS, *et al*. (2010). Preferential associations between co-regulated genes reveal a transcriptional interactome in erythroid cells. Nat Genet 42, 53–61.
Shevtsov SP, Dundr M (2011). Nucleation of nuclear bodies by RNA. Nat Cell Biol 13, 167–173.
Sikorski RS, Hieter P (1989). A system of shuttle vectors and yeast host strains designed for efficient manipulation of DNA in Saccharomyces cerevisiae. Genetics 122, 19–27.
Straight AF, Belmont AS, Robinett CC, Murray AW (1996). GFP tagging of budding yeast chromosomes reveals that protein-protein interactions can mediate sister chromatid cohesion. Curr Biol 6, 1599–1608.
Tan-Wong SM, Wijayatilake HD, Proudfoot NJ (2009). Gene loops function to maintain transcriptional memory through interaction with the nuclear pore complex. Genes Dev 23, 2610–2624.
Thompson M, Haeusler RA, Good PD, Engelke DR (2003). Nucleolar clustering of dispersed tRNA genes. Science 302, 1399–1401.
Weber SC, Brangwynne CP (2015). Inverse size scaling of the nucleolus by a concentration-dependent phase transition. Curr Biol 25, 641–646.
Zenklusen D, Larson DR, Singer RH (2008). Single-RNA counting reveals alternative modes of gene expression in yeast. Nat Struct Mol Biol 15, 1263–1271.
Zhang D, Bai L (2016). Interallelic interaction and gene regulation in budding yeast. Proc Natl Acad Sci USA 113, 4428–4433.
Zhang H, Elbaum-Garfinkle S, Langdon EM, Taylor N, Occhipinti P, Bridges AA, Brangwynne CP, Gladfelter AS (2015). RNA controls PolyQ protein phase transitions. Mol Cell 60, 220–230.
Zhu L, Brangwynne CP (2015). Nuclear bodies: the emerging biophysics of nucleoplasmic phases. Curr Opin Cell Biol 34, 23–30.
Zimmer C, Fabre E (2011). Principles of chromosomal organization: lessons from yeast. J Cell Biol 192, 723–733.
Zullo JM, Demarco IA, Pique-Regi R, Gaffney DJ, Epstein CB, Spooner CJ, Luperchio TR, Bernstein BE, Pritchard JK, Reddy KL, Singh H (2012). DNA sequence-dependent compartmentalization and silencing of chromatin at the nuclear lamina. Cell 149, 1474–1487.